ARTICLE

A Printable Thermally Activated Delayed Fluorescent Polymer Light Emitting Diode

Received 00th January 20xx,
Accepted 00th January 20xx

DOI: 10.1039/x0xx00000x

Cameron M. Cole,[a,b] Susanna V. Kunz,[a,b] Paul. E. Shaw,[c] Nico-Patrick Thoebes,[d] Thomas Baumann,[d] Eva Blasco,[e] James P. Blinco,[a,b] Prashant Sonar,[a,b] Christopher Barner-Kowollik*[a,b] and Soniya D. Yambem*[a,b]

Amongst emissive materials for organic light emitting diodes (OLEDs), thermally activated delayed fluorescent (TADF) materials have shown substantial promise in the last few years. For OLEDs, solution processable and printable emissive materials are highly desirable as printing allows for precise patterning without masks, enables deposition of nanometer scale thicknesses and results in minimal wastage of material. Herein, we introduce a solution processable TADF emitting polymer as an emissive material for OLEDs. The bespoke polymer structure features the TADF emitter 4-(9H-carbazol9-yl)-2-(3'-hydroxy-[1,1'- biphenyl]-3-yl)isoindoline-1,3-dione as a pendant group on a poly(methyl methacrylate) based polymer chain. The resulting OLEDs have a peak emission wavelength of 520 nm with a maximum luminance of around 4700 cd m^{-2}. The peak emission wavelength can be blue-shifted by exciplex management to achieve a peak wavelength of 494 nm. Critically, we employed the TADF-containing polymer system to ink-jet print OLEDs, demonstrating that such polymers are viable for printable OLEDs.

Introduction

Thermally activated delayed fluorescent (TADF) materials for organic light emitting diodes (OLEDs) have attracted considerable attention over the past few years.[1] One of the highly desirable attributes for TADF materials is their ability to harvest 100% of the electrogenerated excited states (excitons) without the use of heavy-metal complexes.[2-4] This advantageous property places TADF materials ahead of their phosphorescent counterparts in terms of their sustainability, which in turn, may facilitate the large-scale fabrication of OLEDs for applications such as display technology and general lighting.[5] The conclusions section should come in this section at the end of the article, before the acknowledgements.

Classically, OLEDs with TADF emitters are fabricated using vacuum deposition. Vacuum deposition, whilst resulting in highly efficient OLEDs, is challenged by a large amount of wastage, chamber size and patterning using masks.[6] An alternative technique to vacuum deposition is solution-processing. Typically, solution-processing is achieved by spin-coating, which is a fast and facile process. In spite of its simplicity, spin-coating results in a large amount of material wastage and the coated film cannot be patterned. For these reasons, the applications for spin-coated OLEDs are limited. An alternative form of solution-processing that solves these issues associated with spin-coating is ink-jet printing.[7]

Ink-jet printing deposits picolitre size droplets of a functional material in any 2D patterned design. This quality, in conjunction with the ability to print various materials at once, enables ink-jet printed OLEDs to have high-resolution and multi-coloured. The majority of the optimization required to produce picolitre size consistent droplets is achieved through extensive ink-engineering.[7,8] Importantly, the viscosities of these inks needs to be higher than spin-coating inks. However, obtaining high viscosities can be problematic for TADF materials, in particular small-molecule TADF materials that are generally insoluble at higher concentrations due to crystallization. Thus, there are very few reports of printable TADF OLEDs. [9-11] A possible route to a functional printable material is designing a polymer emissive material, as emissive polymers enable easier solution-processability.[12]

Herein, we report a solution processable TADF polymer as an emissive material for OLEDs. The bespoke polymer structure features the TADF emitter 4-(9H-carbazol9-yl)-2-(3'-hydroxy-[1,1'- biphenyl]-3-yl)isoindoline-1,3-dione (**E1**) as a pendant group on a poly(methyl methacrylate) (PMMA) based polymer chain. The incorporation of the TADF emitter into a polymer chain increases the viscosity of the ink without increasing the concentration of the TADF emitter. To the best of our

[a.] *Centre for Materials Science, Queensland University of Technology (QUT), 2 George Street, Brisbane, 4000 QLD, Australia.*
[b.] *School of Chemistry and Physics, Queensland University of Technology (QUT), 2 George Street, Brisbane, 4000 QLD, Australia.*
[c.] *Centre for Organic Photonics & Electronics, The University of Queensland, Brisbane, QLD 4072, Australia.*
[d.] *Cynora GmbH, Werner-von-Siemens-Straße 2-6, 76646 Bruchsal, Germany.*
[e.] *Macromolecular Architectures, Institute for Technical Chemistry and Polymer Chemistry, Karlsruhe Institute of Technology (KIT), Engesserstr. 18, 76128 Karlsruhe, Germany.*
[f.] *Institute of Nanotechnology, Karlsruhe Institute of Technology (KIT), Hermann-von-Helmholtz-Platz 1, 76344 Eggenstein-Leopoldshafen, Germany.*
Electronic Supplementary Information (ESI) available. For ESI see DOI: 10.1039/x0xx00000x

knowledge, the herein reported data constitute the first report of ink-jet printed TADF polymer OLEDs.

Experimental Section

OLED fabrication and testing

OLEDs were fabricated on substrates with 80 nm thick pre-patterned ITO (Kintec). The substrates were cleaned by firstly, wiping the sides with acetone, then ultra-sonicated in Alconox and de-ionised water for 10 minuets. Next, the slides were wiped again using Alconox and then ultra-sonicated in de-ionised water, followed by acetone and then isopropanol each for 10 minutes before finally being blow dried with compressed air. The cleaned substrates were spin coated with filtered (0.45μm PVDF filter) PEDOT:PSS (Heraeus) at 5000 rpm for 30 seconds using a Laurell Technologies spin coater, resulting in a thickness of close to 30 nm of PEDOT:PSS. The contact pads were then cleaned of PEDOT:PSS with de-ionised water and then the substrates were annealed at 125°C for 20 minutes.

Standard OLEDs

Following the annealing of PEDOT:PSS film, the substrates were moved into a low oxygen and low moisture glove box (O2 < 10 ppm, H2O < 0.1 ppm) system to complete the fabrication and testing process. They were then spin coated with a solution of **P5**:26DczPPy (30 wt% **P5**) in Chlorobenzene at 1500 rpm for 30 seconds using a Specialty Coating Systems spin coater to achieve a thickness of 30 nm. To prepare the solution of P5:26DczPPy (30 wt% **P5**), individual solutions of **P5** and 26DczPPy were first prepared in Chlorobenzene with a concentration of 10 mg ml^{-1} for both solutions. They were then heated to 100°C for 30 minutes, stirring at 800 rpm. The solutions were then left to stir until cooled down to room temperature, followed by filtering (0.22 μm PTFE filter) and mixing to get the intended ratios of **P5**:26DczPPy. Following the spin coating of EML, the contact pads were cleaned of any EML material using Chlorobenzene and then annealed for 20 minutes at 100°C. They were then loaded into a torpedo thermal evaporator to deposit the remaining layers of TPBi (LumTec), Ba (Sigma Aldrich) and Ag (Sigma Aldrich). These films were deposited at vacuum chamber pressure of ~10^{-6} mbar. The evaporated TPBi, Ba and Ag had a thickness of 20 nm, 10 nm and 100 nm Ag, respectively. The completed standard devices had a pixel size of 2 mm^2.

Current-Voltage-Luminance (IVL) measurements of the OLEDs were done using a B1500A semi-conductor analyser (Keysight) and a calibrated photodiode. The photodiode was calibrated using a luminance meter (CS-200, Konica Minolta). Electroluminescence spectra were recorded using a UV-Vis Spectrometer (USB 2000+, Ocean Optics).

Ink-jet printed OLEDs

All steps of fabrication and testing of the ink-jet printed OLED were done in the same way as those of the standard OLEDs, except for the ink-jet printing of the EML layer. Following the annealing step of PEDOT:PSS, EML were printed using a piezoelectric drop on demand Jet-Lab 4XL ink-jet printer (MicroFab), located outside the glove box system. The solutions/inks for printing were prepared the same as the spin coated inks, however, using 95 vol% anisole and 5 vol% propylene carbonate as the solvents and at a concentration of 10 mg ml^{-1}. The inks were all prepared inside a glove box. The printing of the EML was done as drop on demand with one jet resulting in an average print time of 13 minutes for each OLED print area of 9 mm^2 and approximately 12.5±1.7 nL of ink per OLED, which equates to 0.12 μg of material for the print area of the OLED. The print head was set to a constant 30°C and the print bed at 50°C. The droplets were traveling around 2.86±0.07 mm s^{-1}. Once the EML was printed it was then moved into the glove box system to complete fabrication and testing.

P1 OLEDs

All fabrication steps are the same as that of standard OLEDs, except that (a) individual solutions of **P1** and 26DczPPy in chlorobenzene had a concentration of 20 mg ml-1 and (b) the EML films were spin coated at 1500 rpm to get a thickness 80 nm.

Film characterization

All the samples for the photoluminescent (PL), ultraviolet-visible absorption (UV-Vis), time resolved photoluminescent (TRPL) and photoluminescent quantum yield (Φ_F) were prepared on quartz substrates through spin coating, with the exception of the sample for ΦF which was prepared through drop-casting. The PL measurements and the UV-Vis measurements were recorded using an Agilent fluorescence spectrometer (Cary Eclipse) with an excitation wavelength of 290 nm, and an Agilent UV-Vis (Cary 60), respectively. Time correlated single photon counting (TCSPC) was used to measure the TRPL. A Fluorolog steady state and lifetime modular spectrometer (Horiba), using a pulsed LED emitting at 372 nm was used to photo-excite the films. The films were under vacuum (~10^{-5} mbar) to prevent triplet quenching due to oxygen. Optical filters were used to prevent scattered excitations reaching the detector, which was detecting photoluminescence at 485 nm. Post measuring, the TRPL data was fitted using the sum of 3 exponential (prompt and delayed components).

The film ΦF values were measured using the method described by Greenham et al.[13] The 325 nm output of a He–Cd laser was attenuated with neutral density filters and used to photoexcite the film samples inside an integrating sphere. The interior of the sphere was flushed with nitrogen for the duration of the measurements. The PL signal was measured with a calibrated photodiode with the signal measured at 4 points on each film.

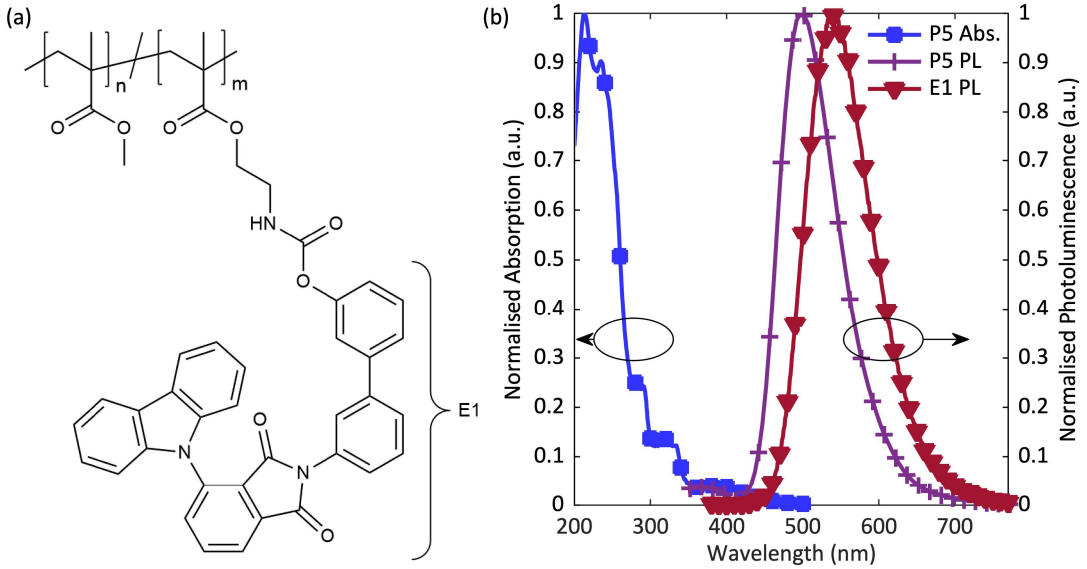

Figure 1. (a) Structure of TADF polymer with a PMMA backbone and TADF emitter **E1** as pendants on the PMMA chain. (b) Solid state UV-Vis absorption spectrum of **P5** and PL spectra of **P5** and **E1**. **P5** is a polymer with structure in (a) with n=95% and m=5% and has M_n = 6800 gmol^{-1} , Đ=1.62.

Duplicate samples were measured with the quoted values the average from 8 measurements (4 per film).

The film samples for fluorescence and phosphorescence measurements were prepared on quartz substrates through spin coating. Films were placed in a nitrogen flushed cuvette for room temperature (RT) measurements and in a glass dewar flask filled with liquid nitrogen for low measurements at 77 K. The low temperature measurements were performed with a 100 ms delay after flash excitation and a 40 ms gate window for signal detection to measure the phosphorescence signal. The excited state energies of the lowest excited singlet and triplet state were determined from the onset of the luminescence spectra at RT and at 77 K, respectively. For that purpose, a tangent was fitted to the high energy side of the spectra at half maximum. The intersection of the tangent with the baseline was taken as onset energy.

The confocal images were taken using a Tescan MIRA3 at 10x magnification and a 488 nm laser to excite the thin films. Topographical images, the surface roughness and the height variations of the printed droplet were recorded using a Bruker Dimension Icon AFM and the analysis program Nano Scope Analysis (Bruker). The film thicknesses were determined using a Bruker Dektak stylus profiler.

Ink viscosity measurements

The viscosity measurements were conducted using an Anton Parr M302 rheometer. The measuring system used was a double gap DG26. The concentration used for the viscosity is 10 mg ml^{-1} is 95 vol% anisole and 5 vol% propylene carbonate. The viscosity was measured with both a consistent (10 s^{-1}) and varying (10 s^{-1} to 1000 s^{-1}) sheet rate, with 20 and 100 data points respectively.

Results and Discussion

Polymer Design

The structure of our TADF polymer with **E1** as a pendant group on a PMMA based polymer chain is shown in **Figure 1a**. The PL spectrum of pure **E1** is depicted in **Figure 1b**, featuring a peak wavelength at 539 nm. To determine the optimal ratio of **E1** to PMMA, a number of thin-film PL measurements (shown in **Figure S1**) were taken using different ratios of PMMA mixed with **E1**, prior to the synthesis of the polymer. There is a clear trend that the PL is red-shifted when increasing the wt% of **E1**. This red-shift in peak PL wavelengths indicates strong aggregation induced concentration quenching with a higher percentage of **E1**, which is common in TADF small molecules.[14] Even though the least amount of aggregation occurs for the lowest wt% of **E1** (Figure S1), a polymer with very low wt% of **E1** would result in excessively large amounts of PMMA in the EML (emissive layer) of the OLED leading to a more insulating emissive layer. To achieve a balance, 5 mol% of **E1** was selected during polymer synthesis affording **P5**. The PL of polymer **P5**, which contains 5 mol% of **E1** in PMMA, is depicted in Figure 1b, featuring a peak PL wavelength of 499 nm. The polymer synthesis is detailed in the Supporting Information Polymer synthesis section.

Photophysical Properties

For a TADF process to occur, the energy gap between the lowest lying triplet energy level (T1) and the lowest lying singlet energy level (S1) need to be small to enable the reverse intersystem crossing (rISC) from T1 up to S1.[1] In order to determine if **P5's** energy gap between S1 and T1 (Δ_{EST}) is sufficiently small to enable the TADF process, temperature-dependent PL measurements were recorded at ambient temperature and at 77K (**Figure 2a**). The S1 and T1 values were determined from the

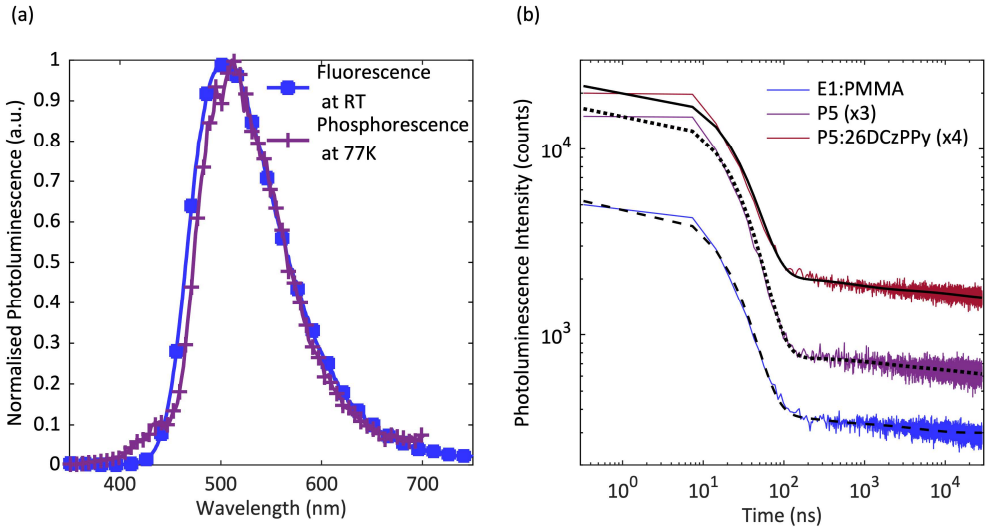

Figure 2. (a) Fluorescence spectra of **P5** taken at ambient temperature and phosphorescence spectra of **P5** taken at 77K. (b) TRPL decay curves of **E1**(5wt%):PMMA, **P5**, and **P5**(30wt%):26DCzPPy. With the fits to the TRPL curves (**E1**(5wt%):PMMA (dash), **P5** (dots), and **P5**(30wt%):26DCzPPy (line). **P5** TRPL data is multiplied by 3 and **P5**:26DCzPPy is multiplied by 4 for clarity.

onset of the fluorescence spectrum at ambient temperature and the phosphorescence spectrum at 77K, respectively (**Table 1**). The Δ_{EST} for **P5** is 50meV, which is within the range for the TADF process to occur.

A small energy gap of Δ_{EST} is a fundamental feature for a TADF system to work. However, it does not prove that there is a delayed fluorescence component. To confirm that the TADF properties are still present in the **P5** polymer, TRPL measurements were conducted for **E1** in PMMA, **P5** and **P5** mixed in 2,6-bis(3-(carbazol-9-yl)phenyl)pyridine (26DCzPPy), which is a commonly used host material in blue OLEDs. **E1** is susceptible to strong concentration quenching, as shown in Figure S1, where the peak PL wavelength for **E1** is red-shifted by ~40 nm as compared to the peak PL wavelength of 5 wt% **E1** in PMMA. Therefore, **E1**:PMMA instead of pure **E1** is used in TRPL measurements to reduce the concentration quenching. Further, 26DCzPPy was chosen as the host material for its highest occupied molecular orbital (HOMO) and the lowest unoccupied molecular orbital (LUMO) values being appropriate for **P5**. 26DCzPPy has a HOMO and LUMO of -6.05 eV and -2.56 eV, respectively, and **P5** has a HOMO and LUMO of -6.13 eV and -3.29 eV, respectively.[15,16] Although 26DCzPPy has a HOMO and LUMO that is acceptable for **P5**, it has a lower triplet energy of 2.71 eV compared to **P5**, which has a triplet energy of 2.72 eV. Ideally, triplet energy level of host should be greater than triplet energy of dopant to reduce transfer of charges from the emitter (dopant) to the host.[17] Whilst the triplet energy level of 26DCzPPy is not ideal, we have chosen it for our devices because there is a limited number of commercially available host materials that could be used in the same solvents with the dopant **P5** and soluble in solvents suitable for ink-jet printing of the emissive layer.

The decay curves for TRPL measurements for all three materials **E1**:PMMA, **P5** and **P5**:26DCzPPy, are shown in **Figure 2b** with their corresponding multi-exponential fits. In all three cases, there are clear and distinct prompt and delayed fluorescence components present in the decay, which shows that the TADF process is present after polymerization to **P5** and when **P5** is mixed with the host material. The prompt and delayed fluorescence decay lifetimes derived from fitting to the room temperature data are provided in Table 1, where all prompt fluorescence decay times (τ_{PF}) are in ns range and all delayed fluorescence decay times (τ_{DF}) are in µs range.

Whilst it is important to have a small Δ_{EST} value for the polymer, it is equally critical to achieve a higher Φ_F, which is often difficult to accomplish when decreasing the Δ_{EST}.[18] To determine the Φ_F and characterise the TADF mechanism in the system, Φ_F measurements were conducted. **E1**:PMMA has a Φ_F of ~46.4 ± 3.9% (Table 1) and **P5** has a Φ_F of ~38.0 ± 2.0%, which is comparable to many TADF polymers with only a few cases exceeding 50%.[12,19] The slight reduction in the Φ_F from **E1**:PMMA to **P5** could be due to an increase in **E1** concentrations and thus an increase in aggregation between the **E1** molecules as shown in Figure S1.[14] The Φ_F increases to ~43.8 ± 2.3% when **P5** is mixed in the host, indicating a reduction in aggregation and the effectiveness of the host material chosen. Prompt fluorescence and delayed fluorescence quantum yield components calculated from the Φ_F and TRPL data (Table 1) show that the prompt fluorescence quantum yield (Φ_{PF}) does not change between the **E1**:PMMA and **P5**:26DCzPPPy and a small increase for **P5**. The ΦPF for **E1**:PMMA, **P5** and **P5**:26DCzPPy being 5.0 ± 0.5 %, 7.4 ± 0.8 % and 5.2 ± 0.4%, respectively.[17] The delayed component of quantum yield (Φ_{DF}), however, follows the trend of total Φ_F. The calculated rate coeffients, krISC, for rISC for **E1**:PMMA, **P5** and **P5**:26DCzPPy are provided in Table 1. The krISC of $3.2 \cdot 10^5 \pm 0.3 \cdot 10^5$ s-1 for **P5** is lower than krISC of $5.4 \cdot 10^5 \pm 0.6 \cdot 10^5$ s-1 for **E1**:PMMA, in spite of smaller Δ_{EST} for **P5** and is highest for **P5**:26DCzPPy with krISC of $5.9 \cdot 10^5 \pm 0.5 \cdot 10^5$ s-1. Further, the T1 energy of **P5** is high (Table 1), which would significantly suppress the non-radiative decay from T1 to the ground state which is important in TADF material.[17] The equations used for the calculations in Table 1 can be found in the Supporting Information section Photophysical calculations.

Table 1: Properties of **E1**, **P5**, and **P5** in 26DCzPPy.

	PL peak [nm]	*HOMO/ LUMO [eV]*	*S1/T1 [eV]*	*ΔE_{ST} [meV]*	*τ_{PF}[ns] /τ_{DF} [µs]*	k_{rISC} *[s^{-1}]*	*Φ_F [%]*	*Φ_{PF}/Φ_{DF} [%]*
E1:PMMA[a]	488	-6.00/ -3.14[c 16]	2.86/ 2.79[d]	70[d]	20.9±0.1/ 17.3±0.8	$5.4\times10^5\pm 0.6\times10^5$	46.4 ± 3.9	5.0±0.5 / 41.4±3.5
P5	499	-6.13/ -3.29[e 16]	2.77/ 2.72	50	23.8±0.1/ 16.3±1.7	$3.2\times10^5\pm 0.3\times10^5$	38.0 ± 2.0	7.4±0.8 / 30.6±1.8
P5: 26DCzPPy[b]	495	-	-	-	24.4±0.2/ 14.5±0.3	$5.9\times10^5\pm 0.5\times10^5$	43.9 ± 2.3	5.2±0.4 / 38.7±2.0

[a] 5wt%**E1** in PMMA; [b] 30wt% **P5** in 26DCzPPy; [c] 1 mol% with 400 mg of Tetrabutylammonium hexafluorophosphate (TBAPF6); [d] 10wt% **E1** in PMMA; [e] 6 mg with 400 mg TBAPF6

OLED Performance

To study the characteristics of **P5** when incorporated in an OLED, OLEDs with a spin coated **P5**: 26DCzPPy emissive layer were investigated using the device structure shown in Figure 3a, which will be referred to as the standard device structure hereafter. The components of the device structure were selected based on the energy levels of **P5** and the host, 26DCzPPy. Poly(3,4-ethylenedioxythiophene)-poly(styrenesulfonate) (PEDOT:PSS), which has a work function of 5.2 eV was selected as the hole transport layer (HTL).[20] PEDOT:PSS is extensively used in solution processed OLEDs and is immiscible in most organic solvents employed for processing of the emissive layer. For the electron transport layer (ETL), a very commonly used ETL, 1,3,5-tris(1-phenyl-1Hbenzimidazol-2-yl)benzene (TPBi) (HOMO/LUMO of -2.8/-6.2 eV) was selected. The device is completed using a Ba/Ag cathode with a work function of -2.7 eV.[21]

The electroluminescence (EL) spectrum, current density and luminance with respect to voltage (IVL) and current efficiency (CE) with respect to luminance for the best standard OLED are shown in **Figure 3b, 3c and 3d**, respectively. The standard OLED turns on at ~ 8.1 V and reaches a maximum luminance of 4697 cd m^{-2}, with a maximum current efficiency (CE) of 4.46 cd A^{-1} and external quantum efficiency (EQE) of 1.05%. The average performance of the standard OLEDs are collated in **Table S2**. A

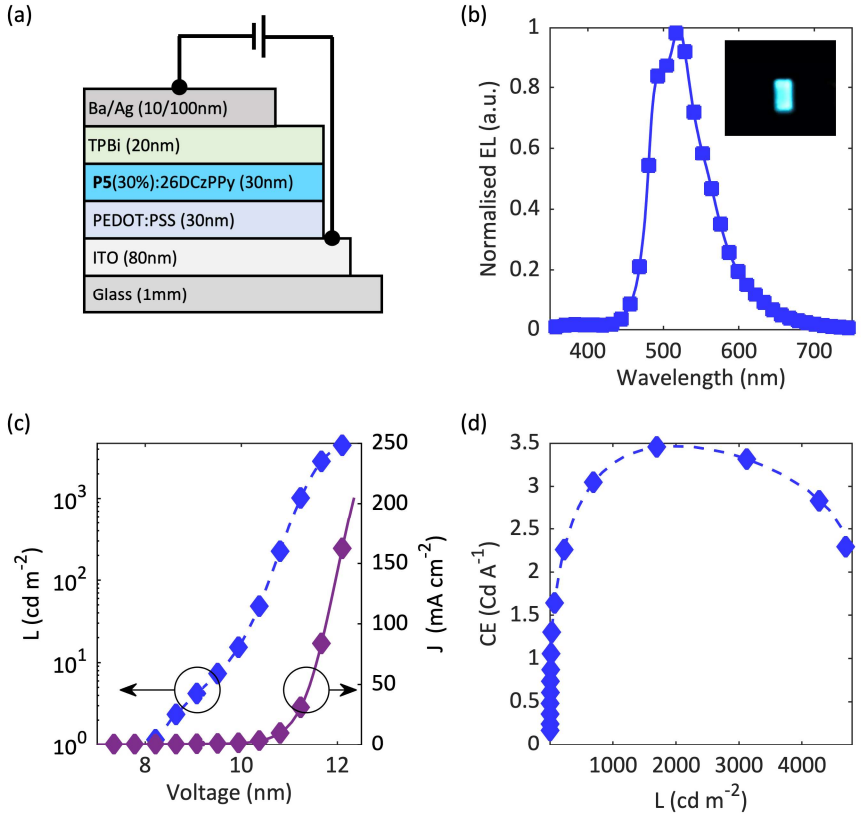

Figure 3. (a) Device structure of our OLED, which we have chosen as a standard device structure of our study. (b) EL spectrum of an OLED with the standard device structure in (a) (the commission Internationale de L'Eclairage coordinates (CIE): 0.26, 0.54). Inset shows photograph of an OLED, (c) Current density and luminance with respect to voltage and (d) current efficiency with respect to luminance of OLED in (a).

comparison of the EL spectra between the standard TADF polymer OLED and a blend-based OLED is also shown in Figure S3. The blend-based OLED has the same device structure as the standard TADF polymer OLED, except for the emissive layer which is in non-polymer form (PMMA:**E1**:Host as emissive layer). It is evident that there is no shift in the peak of EL and there are only a minor differences in the spectra which can be attributed to the difference between the polymeric and non-polymeric emissive layers.

In all the standard OLEDs tested, the EL spectrum contains two distinctive peaks in the emission (Figure 3b), a main peak at 520 nm and a second peak at 495 nm. Compared to the peak PL wavelength of **P5**:26DCzPPy (Table 1) which is 495 nm, the main EL peak is red-shifted by close to 25 nm. Typically, the EL of an OLED does not shift by 25 nm compared to the PL, unless there are other mechanisms of emission other than direct emission from the emitting material, which in our case is **P5**. On the other hand, the second EL peak is at the same peak as the PL, suggesting the second peak is more likely the pure emission from **P5**. To understand the cause of the double peak in EL, devices with different thickness ratio of EML to ETL, whilst keeping the total thickness of EML and ETL constant, were fabricated to adjust the charge recombination zone. ELs for these devices are shown in **Figure S4**, which shows two prominent peaks present in all the devices. The change in the EML:ETL thickness ratios changed the intensity of the two peaks, yet did not change the position of the peaks with 520 nm peak always being the prominent peak. Such observations have been reported earlier as a characteristic of exciplex emissions, indicating exciplex emissions are present in our standard OLED emission.[22,23]

Earlier reports have shown that 26DCzPPy and TPBi both can form exciplexes with other layers next to it.[24,25] To assess if exciplex formation occurs between 26DCzPPy and TPBi, an 'emitter free' version of the standard device (containing no **P5**) was fabricated and found to have strong emission peaks around 520 nm and 490 nm, where the PL of 26DCzPPy does not emit, and reaches a maximum luminance of around 1100 cd m^{-2} (**Figure S5**). This suggests that the EL of standard OLED (Figure 3b), which has a shoulder at ~ 490 nm and peak at ~ 520 nm, have contributions from an exciplex emission formed between 26DCzPPy and TPBi. Furthermore, TPRL measurements were carried out focusing on emission at 500 nm for a blended 26DCzPPy:TPBi film, demonstrated to have a prompt emission followed by a delayed emission in the 100 ns range that would agree with the formation of an exciplex (**Figure S6a**). Exciplex systems having a longer lifetime as a result of the interaction between two materials and forming a CT state. In addition, TPBi and 26DCzPPy do not emit strongly at 500 nm (**Figure S6b**), further suggesting that the emission is due to exciplex and not due to strong prompt emission from either of the two materials.[24,25]

To eliminate the exciplex emission seen in the standard OLEDs, OLEDs with the same structure as standard OLEDs (Figure 3a)

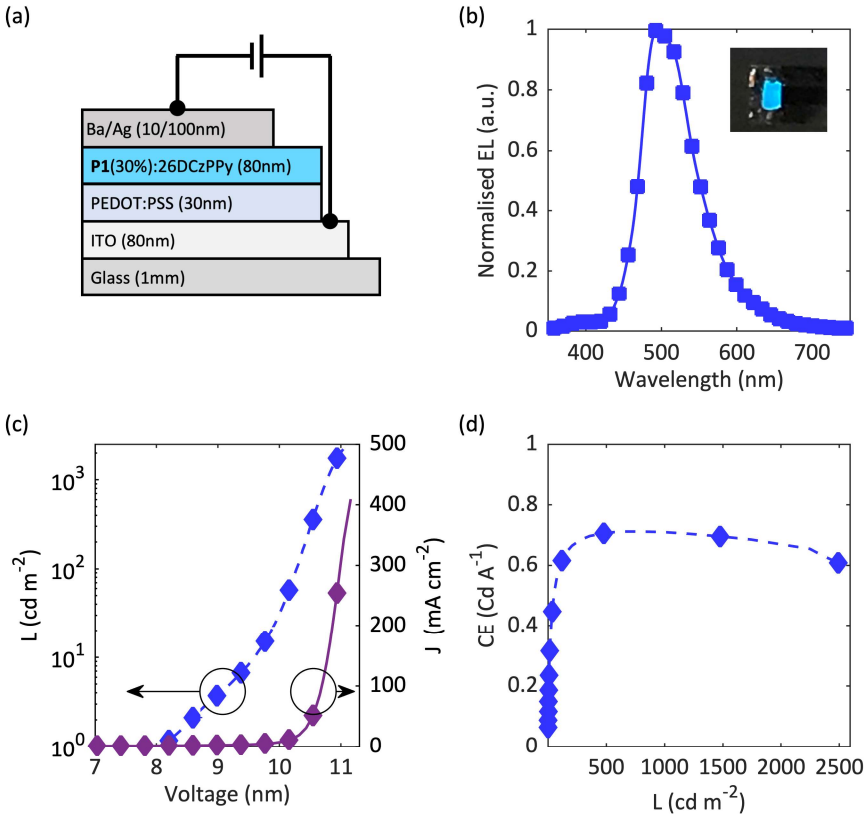

Figure 4. (a) Device structure of OLED with **P1** in EML. Note: There is no TPBi layer in this structure. (b) EL spectrum of the **P1** OLED (CIE: 0.22 0.46). Inset shows photograph of an OLED. (c) Current density and luminance with respect to voltage. (d) Current efficiency with respect to luminance.

but without TPBi were fabricated. These OLEDs without TPBi had a single peak emission at 512 nm (**Figure S7**), which is still red-shifted compared to PL of **P5**: 26DCzPPy. A possible contribution to the red-shifting of the EL could be the aggregation of the emitter components within the polymer. Therefore, a polymer, **P1**, with only 1 mol% of **E1** was synthesised and OLEDs were fabricated with a structure shown in **Figure 4a**. These OLEDs with **P1** in the EML and without TPBi showed an EL peak at 494 nm (**Figure 4b**), reaching a maximum luminance of ~2500 cd m^{-2} (**Figure 4c**). The maximum luminance, CE (0.24 cd A^{-1}) and EQE (0.71%) of **P1** OLEDs are significantly lesser than the standard OLEDs. However, this is expected since **P1** OLEDs do not have an ETL layer and the EML has less than 2 wt% of **E1**. In these circumstances, the luminance of ~2500 cd m^{-2} shows great promise for further increase in the EQE for the device with the increase of the emitter but without aggregation. Similar to standard OLEDs, exciplex free OLEDs with **P1** have a relatively large turn-on voltage of 8.1V. A significant contribution to the large turn-on voltages of the polymer OLED can be attributed to the large amount of PMMA within the EML. Whilst this is not ideal for an OLEDs performance it is beneficial to improving the printability of the polymer.

Ink-Jet Printed OLED

To demonstrate the printability of OLEDs, polymer **P5** and 26DCzPPy was prepared into an ink in 95 vol% anisole and 5 vol% propylene carbonate at 10 mg mL^{-1}. These two solvents were selected for the ink-jet printing, as they feature low toxicity, making the ink more environmentally friendly for mass scale production. Further, both **P5** and 26DCzPPy are soluble in both the solvents. In addition, the solvents had a sufficiently high viscosity to be a printable ink when the **P5**:26DCzPPy was added to it. Anisole had a viscosity of 1.01 ± 0.01 mPa·s, while a solvent of 95 vol% anisole and 5 vol% propylene carbonate had a viscosity of 1.05 ± 0.01 mPa·s. The **P5**:26DCzPPy ink used for printing had a viscosity of 1.12 ± 0.02 mPa·s (**Figure S8**) and consistent jetting without satellite formation was achieved (**Figure 5a**) .[26] The droplet sizes were approximately 70 µm in diameter. Confocal microscope image of a printed film on PEDOT:PSS is shown in **Figure 5b**. The droplets were separated by ~20µm, which was due to the effect the droplets had on each other when they were closer together. The topographical differences between spin coated and inkjet-printed films of the emissive layer can be seen from the atomic force microscope images shown in **Figure 6**. Both the spin coated and the ink-jet printed films were deposited on PEDOT:PSS layer to reflect the

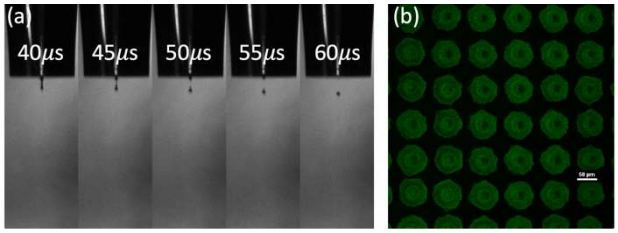

Figure 5. (a) Stroboscopic images of jetting of **P5**:26DCzPPy ink showing consistent jetting where no satellite forms after droplets are formed (b) Confocal images of printed **P5**(30 wt%):26DCzPPy film on PEDOT:PSS.

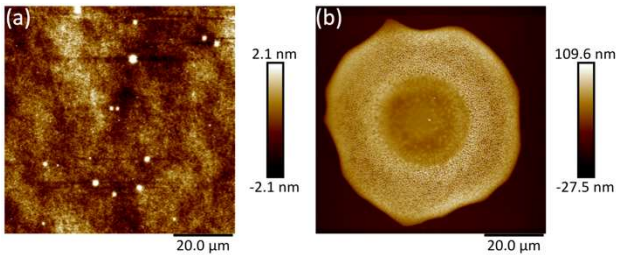

Figure 6. AFM images of (a) spin coated film of **P5**:26DCzPPy in chlorobenzene that was used for the standard OLED on PEDOT:PSS. (b) Ink-jet printed droplet of **P5**:26DCzPPy in 5 vol% propylene carbonate and 95 vol% anisole on PEDOT:PSS.

characteristic of emissive layer films in actual OLEDs. The spin coated film had a root mean square roughness (Rq) of 0.92 nm over 80 µm by 80 µm area (Figure 6a). A cross-sectional profile of the AFM image of a printed droplet shown in Figure 6b, is provided in **Figure S9**. The cross-sectional image shows a minor coffee ring effect, which is a common problem in printed films. Further investigations in printing parameters and ink variations need to be carried out to completely overcome the coffee ring effect.

OLEDs fabricated with a printed EML have the same structure as the standard OLED structure (Figure 3a). The device structure and an image of the printed OLED is shown in Figure 7a. The EL, IVL and CE of the best printed OLED are provided in **Figure 7 b, c and d**. The EL of the printed OLED has two prominent peaks at 490 nm and 522 nm, which is expected since the OLED structure is the standard structure which has exciplex emission. The printed OLED has a turn on voltage of 5.3 V, reaching a maximum of 607 cd m^{-2}, and a maximum CE and EQE of 0.33 cd A-1 and 0.1%, respectively. Compared to the spin coated standard OLED, the performance of the printed OLED is significantly lesser since the printed films are yet to reach the optimum quality. However, the OLED data for printed devices show that our approach to achieve printable TADF materials is a promising strategy towards inkjet printable TADF OLEDs. Reducing surface roughness and achieving a uniform continuous printed film will improve the OLED performance and further research is underway in our laboratories.

Here the highest performing device is reported for the OLED with ink-jet printed EML. The performance of this OLED is significantly less than that of the spin coated film due to the thickness variation in the films where the droplets are 65 nm in height and 40 nm in height in the centre (coffee-ring effect), in addition to there being sections where there is no ink (between droplets) (Figure S9a).

Conclusions

Herein, we report a novel inkjet printable TADF polymer and demonstrate, for the first time, an inkjet-printed TADF polymer OLED. Complete characterization of thin film properties of the TADF polymer and performance of OLEDs using the TADF polymer are carried out. Through temperature dependent PL, TRPL and Φ_F we evidence that the performance of the polymer is similar to the original TADF emitter complex. The rISC and Φ_F values of our TADF polymer are comparable with current TADF polymers, with the additional ability to be ink-jet printable. The

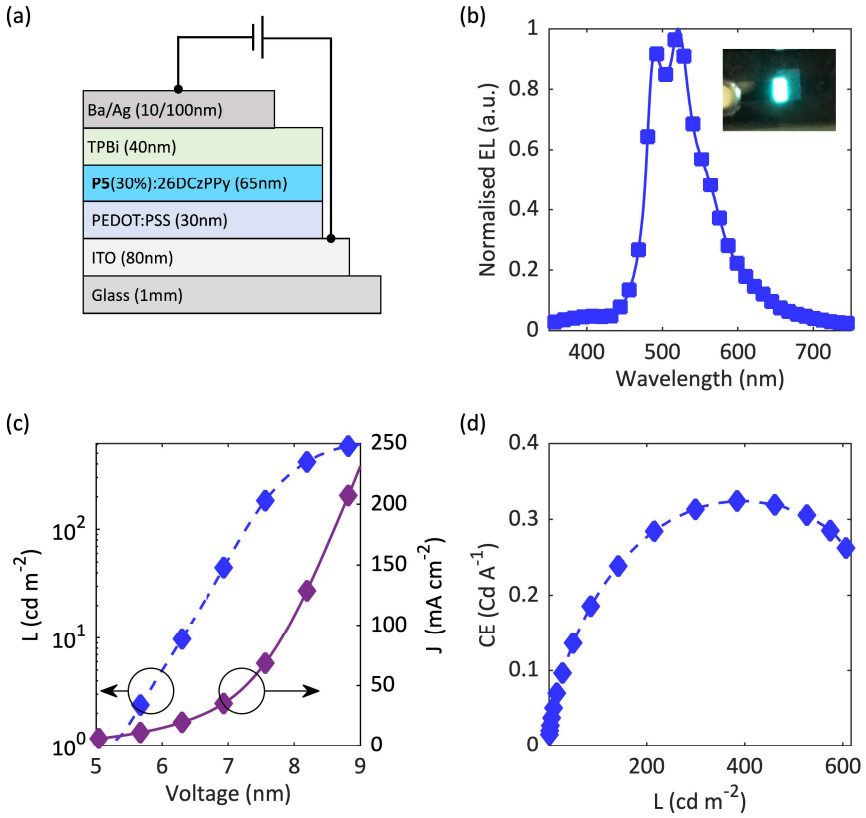

Figure 7. (a) Device structure of ink-jet printed OLED with **P5** in EML. (b) EL spectra of the Printed OLED (CIE: 0.26, 0.51). Insert shows photograph of an OLED, (c) Current density and luminance with respect to voltage. (d) Current efficiency with respect to luminance.

inkjet printability is largely due to the PMMA backbone, which is favourable for printing. The successful fabrication of ink-jet printed TADF OLED shows substantial promise for printable OLEDs and future work will be focused on improvement through the optimization of the printed film. Importantly, strategies to improve the electrical properties of the TADF polymer whilst still maintaining the printable characteristics of the ink, are currently underway.

Conflicts of interest

There are no conflicts to declare.

Acknowledgements

C.B.-K. is grateful for an ARC Laureate Fellowship enabling his photochemical research program as well as continued key support from the Queensland University of Technology (QUT) through the Centre for Materials Science. C.B.-K., J.B., P.S., and S.Y. acknowledge funding in the context of an Australian Research Council (ARC) Linkage project LP160101230. The Central Analytical Research Facility (CARF) at QUT is gratefully acknowledged for access to analytical instrumentation and laboratory space, supported by the Science and Engineering Faculty at QUT. E.B. acknowledges the financial support from the Helmholtz program "Science and Technology of Nanosystems" (STN). P. S. is also thankful to the Australian Research Council (ARC) for the Future Fellowship (FT130101337).

References

1 Z. Yang, Z. Mao, Z. Xie, Y. Zhang, S. Liu, J. Zhao, J. Xu, Z. Chi and M. P. Aldred, *Chem. Soc. Rev.* 2017, **46**, 915.
2 2 A. Endo, K. Sato, K. Yoshimura, T. Kai, A. Kawada, H. Miyazaki and C. Adachi, *Appl. Phys. Lett.* 2011, **98**, 083302.
3 3 Q. Zhang, D. Tsang, H. Kuwabara, Y. Hatae, B. Li, T. Takahashi, S. Y. Lee, T. Yasuda and C. Adachi, *Adv. Mater.* 2015, **27**, 2096.
4 4 A. Endo, M. Ogasawara, A. Takahashi, D. Yokoyama, Y. Kato and C. Adachi, *Adv. Mater.* 2009, **21**, 4802.
5 5 D. Volz, M. Wallesch, C. Flechon, M. Danz, A. Verma, J. M. Navarro, D. M. Zink, S. Brase and T. Baumann, *Green Chem.* 2015, **17**, 1988.
6 6 T. Huang, W. Jiang and L. Duan, *J. Mater. Chem. C* 2018, **6**, 5577.
7 7 F. Villani, P. Vacca, G. Nenna, O. Valentino, G. Burrasca, T. Fasolino, C. Minarini and D. della Sala, *J. Phys. Chem. C* 2009, **113**, 13398.
8 8 I. Burgués-Ceballos, M. Stella, P. Lacharmoise and E. Martínez-Ferrero, *J. Mater. Chem. A* 2014, **2**, 17711.
9 9 A. Verma, D. M. Zink, C. Flechon, J. L. Carballo, H. Flugge, J. M. Navarro, T. Baumann and D. Volz, *Appl. Phys. A: Mater. Sci. Process.* 2016, **122**,
10 10 M. Wallesch, A. Verma, C. Flechon, H. Flugge, D. M. Zink, S. M. Seifermann, J. M. Navarro, T. Vitova, J. Gottlicher, R. Steininger, L. Weinhardt, M. Zimmer, M. Gerhards, C. Heske,

S. Brase, T. Baumann and D. Volz, *Chem. - Eur. J.* 2016, **22**, 16400.
11 11 C. Amruth, B. Luszczynska, M. Z. Szymanski, J. Ulanski, K. Albrecht and K. Yamamoto, *Org. Electron.* 2019, **74**, 218.
12 12 Q. Wei, Z. Ge and B. Voit, *Macromol. Rapid Commun.* 2019, **40**, 1800570.
13 13 N. C. Greenham, I. D. W. Samuel, G. R. Hayes, R. T. Phillips, Y. A. R. R. Kessener, S. C. Moratti, A. B. Holmes and R. H. Friend, *Chem. Phys. Lett.* 1995, **241**, 89.
14 14 H. S. Kim, S.-R. Park and M. C. Suh, *J. Phys. Chem. C* 2017, **121**, 13986.
15 15 Y. S. Tsai, L. A. Hong, F. S. Juang and C. Y. Chen, *J. Lumin.* 2014, **153**, 312.
16 16 S. V. Kunz, C. M. Cole, A. Welle, P. E. Shaw, P. Sonar, N. P. Thoebes, T. Baumann, S. D. Yambem, E. Blasco, J. P. Blinco and C. Barner-Kowollik, *Macromolecules* 2019, **52**, 9105.
17 17 F. B. Dias, T. J. Penfold and A. P. Monkman, *Methods Appl. Fluoresc.* 2017, **5**, 012001.
18 18 P. Rajamalli, N. Senthilkumar, P. Gandeepan, P.-Y. Huang, M.-J. Huang, C.-Z. Ren-Wu, C.-Y. Yang, M.-J. Chiu, L.-K. Chu, H.-W. Lin and C.-H. Cheng, *J. Am. Chem. Soc.* 2016, **138**, 628.
19 19 M. Y. Wong and E. Zysman-Colman, *Adv. Mater.* 2017, **29**, 1605444.
20 20 P VP AI 4083, https://www.heraeus.com/media/media/hec/documents_hec/data_sheets_hep/Clevios_P_VP_AI_4083.pdf, (accessed: March, 2020).
21 21 J. Xing, Y. Zhao, M. Askerka, L. N. Quan, X. Gong, W. Zhao, J. Zhao, H. Tan, G. Long, L. Gao, Z. Yang, O. Voznyy, J. Tang, Z.-H. Lu, Q. Xiong and E. H. Sargent, *Nat. Commun.* 2018, **9**, 3541.
22 22 W. Bernal, O. Barbosa-García, A. Aguilar-Granda, E. Pérez-Gutiérrez, J.-L. Maldonado, M. J. Percino and B. Rodríguez-Molina, *Dyes Pigm.* 2019, 754.
23 23 S. Yang and M. Jiang, *Chem. Phys. Lett.* 2009, **484**, 54.
24 24 D. Chen, Z. Wang, D. Wang, Y.-C. Wu, C.-C. Lo, A. Lien, Y. Cao and S.-J. Su, *Org. Electron.* 2015, **25**, 79.
25 25 X. Ban, K. Sun, Y. Sun, B. Huang and W. Jiang, *ACS Appl. Mater. Interfaces* 2016, **8**, 2010.
26 26 Satellites occurrence and approaches to eliminate them, http://www.microfab.com/images/pdfs/Satellites_version_09_26_07.pdf, (accessed: March, 2020).